Fwd: ApJ96041R2 Decision Letter

andrea costa <acosta@oac.unc.edu.ar>   Mon, May 11, 2015 at 10:35 AM
To: Ernesto Zurbriggen <ernesto.zurbriggen@gmail.com>, matias schneiter <mschneiter@gmail.com>,
Mariana Cecere <marialda27@gmail.com>

---------- Forwarded message ----------
From: <apj@msubmit.net>
Date: 2015-05-11 10:11 GMT-03:00
Subject: ApJ96041R2 Decision Letter
To: acosta@oac.unc.edu.ar
Cc: edeluca@cfa.harvard.edu

May 11, 2015

Prof. Andrea Costa
Instituto de Astronomía Teórica y Experimental IATE - CONICET
laprida 854
córdoba, córdoba 5000
Argentina

Title: 3D MHD Simulation of Flare Supra--Arcade Downflows in a Turbulent Current Sheet Medium,
ApJ96041R2

Dear Prof. Costa,

I am happy to report that the above paper is accepted for publication in The Astrophysical Journal.

I have attached the reviewer's final comments. Please attend to the minor corrections during the final
preparations for publication.

I am sending the accepted version to the ApJ editorial office. Correspondence concerning the logistical
aspects of publishing this manuscript should be directed to apj@apj.usask.ca. If you have any additional
questions concerning the scientific content of your manuscript, please direct them to me.

Sincerely,
Dr. Edward DeLuca
ApJ Scientific Editor
Harvard Smithsonian Center for Astrophysics
edeluca@cfa.harvard.edu

1_reviewer_attachment_2_1430853209_convrt.pdf
61K

3D MHD simulation of flare supra–arcade downflows in a turbulent current sheet medium

M. Cécere[1,2], E. Zurbriggen[1,2], A. Costa[1,2,3], M. Schneiter[1,2,3]

ABSTRACT

Supra–arcade downflows (SADs) are sunward, generally dark, plasma density depletions originated above posteruption flare arcades. In this paper using 3D MHD simulations we investigate if the SAD cavities can be produced by a direct combination of the tearing mode and Kelvin–Helmholtz instabilities leading to a turbulent current sheet (CS) medium or if the current sheet is merely the background where SADs are produced triggered by an impulsive deposition of energy. We find that to give account of the observational dark lane structures an addition of local energy, provided by a reconnection event, is required. We suggest that there may be a closed relation between characteristic SAD sizes and CS widths that must be satisfied to obtain an observable SAD.

Subject headings:

1. Introduction

SAD features are known to be dark moving trails originated $[40 - 60]$Mm above eruption flare arcades with decelerating speeds in the range $\sim [50 - 500]$km s^{-1} (McKenzie 2000; McKenzie and Savage 2009; Savage and McKenzie 2011). They were first detected with the *Yohkoh* Soft X–ray Telescope (SXT) (McKenzie and Hudson 1999). Since then, they have been extensively reported using other instruments such as *TRACE* (Innes et al. 2003a,b), *SOHO*/SUMER (Innes et al. 2003b) and *SDO*/AIA (Savage et al. 2012). There is consensus in that due to the lack of X–ray and extreme–ultraviolet (EUV) signatures in images and spectra, these SAD structures are voided flows generated by reconnection processes in a CS above the flare arcade.

Several scenarios have been proposed to give account of the observations. After new AIA detections with high spatial resolution and temporal cadence, Savage et al. (2012) re-interpreted SADs as density depletions left in the wake of thin shrinking loops. These authors indicated that either retracting loops will be observed, when above the flare arcade is devoid of plasma (impulsive phase), or SADs, when a hot dense fan of plasma is present above the flare arcade (decay phase). They also proposed that deceleration is expected due to the buildup of downstream magnetic pressure and/or drag mechanisms.

Another scenario was proposed by Linton et al. (2009), where the dynamic of retracting magnetic fields is triggered by a localized reconnection event that produces up and down flowing reconnected flux tubes, which are slowed down by underlying magnetic arcade loops. A drawback with this scenario is that the observed SAD speeds are lower than expected for reconnection outflows in regions of typical Alfvén speeds of 1000km s^{-1}.

We are specially interested in the turbulent CS description given by McKenzie (2013). He analyzed high–resolution observations in a sheet–like structure above a post–CME flare arcade where the turbulent dynamic of a complex flow is described. He found that the plasma β (the ratio of gas to magnetic pressure) is of the order of unity and described the flow variability in the hot plasma ($T > 10$MK) as a product of strong velocity shears and vortical motion where small vortices moving towards the arcade were interpreted as probable SAD structures.

In Costa et al. (2009), Schulz et al. (2010), Maglione

et al. (2011) and Cécere et al. (2012) we reproduced the dynamics of multiple decelerating downflows through the assumption that dark tracks are confined voided cavities –of high β and temperature values– collimated in the direction of the ambient magnetic field and, generated by the bouncing and interfering of shocks and expansion waves upstream of the initial localized deposition of energy provided by reconnection events. In this scenario, the different observational SAD sizes could be interpreted either as the consequence of reconnection events that are triggered in a homogeneous background, or as the consequence of reconnection events produced in a previously distorted media by the passage of earlier SADs. We found that the observed wavy character (Verwichte et al. 2005) can be interpreted as an indication of interaction between SADs. This interaction is significant when the bursts that trigger the phenomenon act on the wakes left by previous SADs.

Recent observational data and modeling have challenged the scenario described by Cécere et al. (2012). Hanneman and Reeves (2014) measured the plasma temperature of the SAD regions and surrounding plasma sheet using AIA and XRT data. They calculated differential emission measures for several flares and their corresponding SADs and found that there is little convincing evidence to sustain the high temperatures in the SADs predicted by Maglione et al. (2011) and Cécere et al. (2012). They also found that SADs are always hotter than the background, but in many cases cooler than the surrounding fan plasma.

Related with thermal conduction considerations, one of the major challenges is to understand how it is possible that SADs can last in hot CS. In fact, structures with typical SAD sizes of decades of Mm, typical coronal number densities of $n \approx 10^9 \mathrm{cm}^{-3}$ and temperatures as high as $T \approx 10\mathrm{MK}$ (McKenzie 2013) will vanish in times (of a few seconds) that are at least two orders of magnitude lower than the observed values. However, we show that considering a typical coronal background ($T \sim 1\mathrm{MK}$) or/and the high density fan region ($n \sim 2 \times 10^{10}\mathrm{cm}^{-3}$) as the medium where the SAD dynamic develops, the thermal conduction effects are lower enough to allow the comparison with the observations.

In what follows motivated by the description provided by McKenzie (2013) we explore a new scenario. We consider a quasi–2D turbulent CS as the medium where SAD features can be observed. We propose that SADs are voided cavities formed by nonlinear waves. Waves which are triggered by bursty reconnection events (blast wave expansion mechanism, Forbes (1988); Kumar and Innes (2013)) that occur during a larger scale reconnection process. This is, the quasi–2D turbulent CS evolution times are much larger than the SAD ones. We emulate these individual reconnection events by pressure pulses.

We perform 3D MHD simulations including magnetic resistivity and assuming that heating and cooling terms compensate each other. The paper is structured as follows: In Sec. 2 we consider turbulence and CS formation; in Sec. 3 we justify the assumption made regarding the cooling (conduction and radiation) and heating (reconnection) term; in Sec. 4 we present the model; in Sec. 5 we state the numerical setup and initial conditions. In Sec. 6 we discuss the results obtained and in Sec. 7 we summarize the conclusions.

2. Reconnection processes: turbulent current sheets and bursty reconnection

The notion of quasi–separatrix layers proved to be fertile since observational and theoretical reconnection studies showed that 3D reconnection requires to go beyond the classical generalization of 2D null points and their correspondent separatrices (e.g. Priest and Démoulin (1995); Schmieder et al. (1997)).

However, the study of 2D CS formation and evolution is still important even for 3D calculations. Onofri et al. (2004) simulated magnetic reconnection on a slab geometry and showed that the presence of a global guiding magnetic field makes the 3D evolution much similar to those of purely 2D (see also Fermo et al. (2010)). The formation of smaller scale structures associated with a direct energy transfer, allowing larger diffusion and faster reconnection rates, is a consequence of the nonlinear evolution that eventually ends in a turbulent regime of many spatial scales. The simulations with a guide field produce both, a direct and an inverse energy cascade. The inverse energy transfer generates coalescence of magnetic islands which are typical 2D structures. In the direct cascade the wavelengths decrease with increasing distance from the CS. Coalescence is mostly suppressed when faster 3D phenomena are significative. Thus, the fact that coalescence is present is an indication that a 2D picture is a good description of a phenomenon.

Typical observational evidences of these quasi–2D CS configurations were described by Guo et al. (2013) where the coalescent plasmoids, or those long–lasting

2

slab configurations usually seen above arcades can be observed (e.g. McKenzie (2000); McKenzie and Savage (2009); Savage and McKenzie (2011)).

There is a broad range of determinations concerning the thickness of 2D CS. Guo et al. (2013), based on observational data and using a 2D simulation estimated an upper limit of the CS width of 3Mm. However, associated with non-thermal line widths, Ciaravella and Raymond (2008) reported CS thickness ranging within ~ [28 − 56]Mm and Bemporad (2008) attributed the large temperatures and observed CS thickness (~ [10 − 100]Mm) to turbulence. Discrepancies between widths could be due to, either the impossibility to observationally distinguish between the CS and a sheath of hot plasma surrounding the CS (Seaton and Forbes 2009), to non-thermal bulk flows and/or turbulence (Ciaravella and Raymond 2008; Bemporad 2008) or to different regimes of 2D CSs behavior (Heyvaerts and Kuperus 1978) where an adiabatic description would be accurate.

Deviating from these 2D descriptions, flares that release impulsive energy in absence of a sustained gradual phase were extensively studied (e.g. Priest (1982)). The existence of explosive events in reconnection processes imply that they occur on a faster timescale than large–scale ones. It was suggested that this could be either due to the presence of stressed magnetic flux tubes that become unstable and produce individual bursty reconnection in the frame of the longer term process or because reconnection itself is inherently impulsive and bursty (Priest 1986; Priest and Forbes 2000). Forbes (1988) pointed out the importance of blast waves produced by pressure–driven expansions and shocks due to impulsively driven reconnection, and recently Kumar and Innes (2013) observed a limb flare and proposed a flare blast wave scenario to describe it.

Thus, due to the above discussion we will consider a turbulent quasi-2D CS of different thicknesses as the medium where SADs may be observed.

3. The effects of thermal conduction

Seaton and Forbes (2009) studied a CS model to analyze reconnection outflow jets considering thermal conduction. Based on a model by Somov et al. (1987) they assumed that a 2D CS is generated by a Petschek-type reconnection model and found that, for large heat conduction values, the internal CS temperatures are almost uniform and equal to the background values (see Figure 7 in Seaton and Forbes (2009)). Con-

sidering that surrounding a CS an expanded thermal halo is formed, they assumed an almost steady configuration where, in accordance with observations, density is uniform and internally enhanced over the background coronal densities (Schwenn et al. 2006). However, this CS scenario of almost uniform density and low temperature, dominated by heat conduction, does not seem to be consistent with a typical turbulent inhomogeneous hot media where SADs are observed. It seems that only when conduction is not dominant with respect to the reconnection process (they did not consider cooling by radiation), higher internal CS temperatures and nonuniform density distributions would be obtained.

In fact, Ciaravella and Raymond (2008) studied the CS associated with the 2003 November 4th CME and found large non-thermal [Fe XVIII] line broadening. The corresponding speeds were as high as 380km s^{-1} at an early stage, and later -in a fairly constant phase- they ranged between [50 − 200]km s^{-1}. They concluded that these non-thermal effects are explained by the presence of turbulence and bulk flows.

Although conduction and radiation are both cooling processes, while conduction proceeds to distribute heat –being highly efficient in hot CSs– the radiation acts as a sink function that takes heat away locally. Thus, the heat conduction tends to expand the system distributing the energy, and the radiation tends to narrow it by reducing the gas pressure with respect to the surrounding media. Theoretical and observational CS studies (e.g. Bemporad (2008); Ciaravella and Raymond (2008)) support the existence of CSs with quasi stable thickness values, thus, reconnection processes should provide the energy to stabilize the CS width for times comparable with the observations. Thus, a certain set of CS parameters could give account of an energy balanced open system where diffusion is limited allowing the observation of SADs for times comparable with the observations.

There are three main physical processes for energy balance in the CS: thermal conduction, radiation and reconnection. The timescales of conductive and radiative cooling are:

$$t_{cond} \equiv \frac{3nk_BL^2}{\kappa_0 T^{5/2}}, \quad t_{rad} \equiv \frac{3k_BT}{nE_r}, \quad (1)$$

where n is the number density, k_B is the Boltzmann constant, L is a characteristic length, $\kappa_0 \approx 10^{-6}$erg K$^{-7/2}$ cm^{-1} s^{-1} is the heat conduction coefficient along the magnetic field, T is the temperature and E_r is the

radiative loss function ($E_r \simeq 4 \times 10^{-23}$erg cm^3 s^{-1} for $T \simeq$ 10MK) (Aschwanden 2005).

To evaluate the timescale of reconnection heating, t_{rec}, we follow Lazarian and Vishniac (1999) who proposed a low dissipation model where a turbulent quasi 2D CS is formed due to the presence of a guiding magnetic field that reduces the transverse scale for reconnection flows. Turbulent motion create small regions of intense field gradients and reconnection occurs in small layers spread throughout the larger direction. Associated with their model the reconnection timescale is:

$$t_{rec} \equiv \frac{L}{v_A M_A^2} \qquad (2)$$

where v_A is the Alfvén speed and M_A is the Mach Alfvén number.

Hence, our aim is now to determine realistic CS physical parameters which lead to timescales compatible with an almost non-diffusive description, i.e., where SAD features can develop for times comparable with the observations.

4. The Model: SADs as blast waves explosive events during a long duration reconnection process in a turbulent media

We assume that SADs are voided and expanded cavities resulting from bursty reconnections (Forbes 1988; Kumar and Innes 2013) that occur during a larger scale 2D turbulent CS reconnection process. The triggering blast wave mechanism was proposed in Costa et al. (2009) (see e.g., the explanation given in Cécere et al. (2012) and Figure 3 therein). They are assumed as local features independent of the overall turbulent quasi–2D CS. Thus, they may eventually be triggered outside the CS reconnection region. However, because of the simplicity of the setup used (where the background is not modeled, only the CS environment was used to analyze the dynamic behavior) we can only simulate the case where SADs are triggered (already immersed) inside the CS, but we will argue, in the conclusion section, about what could happen when they are triggered outside the CS (see Figure 1).

The initial conditions for the chosen CS parameters are: an average temperature value of $T =$ 10MK, an initial sunwardly guiding magnetic field value of $B =$ 5.9G (y axis), and an enhanced CS number density value of $n = 2 \times 10^{10}$cm^{-3}. As heat conduction is strongly inhibit across the magnetic field lines, and considering that the guiding magnetic field is ori-

ented in the y direction we calculate the heat conduction timescale considering a typical CS length of $L =$ 140Mm. With these values and using Eq. (1) we obtain: $t_{cond} \simeq t_{rad} \simeq$ 5100s.

With the above CS parameters, the Alfvén speed results $v_A =$ 92km s^{-1} and, considering an average turbulent speed of $v =$ 50km s^{-1} ($M_A \sim$ 0.5) (Ciaravella and Raymond 2008; McKenzie 2013), using Eq. (2) we obtain $t_{rec} \simeq$ 5247s.

If we consider that a typical SAD is triggered by a blast phase associated with an initial adiabatic expanding shock, thermal conduction will not play a significant role in the exchange of heat with the surroundings at this early stage. Later, the thermal exchange with the SAD neighborhood will strongly depend on the field orientation. The blast stage leads to a magnetic configuration where the magnetic field lines tend to displace and envelope the SAD, thus the tendency is to thermally insulate it from the surroundings. Meanwhile, considering that SADs travel $\sim (20 - 40)$Mm along the sunward y direction (appearing as elongated feature of $\sim$ 40Mm in the fan region) we respectively obtain: $t_{cond} \simeq (105 - 400)$s, which is consistent with observational times. See e.g., the movies provided by Savage et al. (2012).

With these assumptions, taking into account the calculated timescales, we consider that the cooling and heating terms compensate each other and that the conduction will not substantially alter the results for times comparable with the SAD observations. Different values of the chosen physical parameters would lead to a different scenario. In favour of this one we can argue that lower thermal conduction times associated with other realistic set of parameters would lead to a rapid extinction of the observed features. We speculate that this particular scenario could explain why SADs are not always observed associated with supra–arcade CSs. A model considering cooling terms due to anisotropic thermal conduction, radiation, and reconnection heating is in progress.

5. Numerical code and initial conditions

We numerically solve the MHD equations. In conservative form they read (CGS units):

$$\frac{\partial \rho}{\partial t} + \nabla \cdot (\rho \mathbf{v}) = 0, \qquad (3)$$

$$\frac{\partial \rho \mathbf{v}}{\partial t} + \nabla \cdot (\rho \mathbf{v}\mathbf{v} - \mathbf{B}\mathbf{B}) + \nabla p_* = 0, \qquad (4)$$
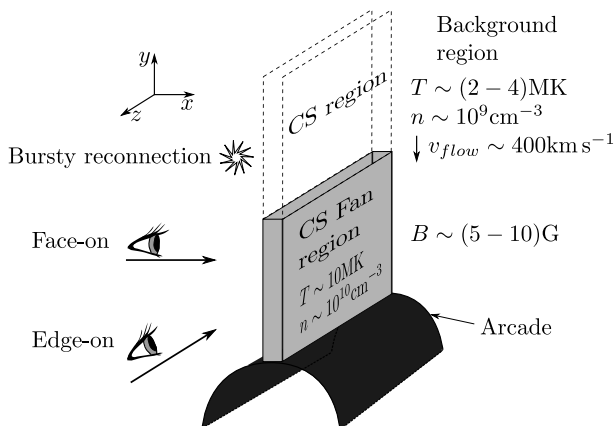
4

Fig. 1.— Simplified scheme of the 2D CS, formed by stochastic reconnection (Lazarian and Vishniac 1999), immersed in a coronal background media. A blast-wave reconnection process (Kumar and Innes 2013) leading to the formation of a SAD, is also indicated.

$$\frac{\partial e}{\partial t} + \nabla \cdot [(e + p_*)\mathbf{v} - \mathbf{B}(\mathbf{v}.\mathbf{B})] =$$

$$\nabla \cdot [\mathbf{B} \times (\eta \nabla \times \mathbf{B})], \quad (5)$$

$$\frac{\partial \mathbf{B}}{\partial t} + \nabla \cdot (\mathbf{v}\mathbf{B} - \mathbf{B}\mathbf{v}) = \eta \nabla^2 \mathbf{B}, \quad (6)$$

$$e = \frac{1}{2}\rho v^2 + E + \frac{B^2}{2}, \quad (7)$$

$$p_* = p + \frac{B^2}{2}, \quad (8)$$

$$p = (\gamma - 1)E, \quad (9)$$

where ρ is the mass density, t is the time, $\mathbf{v}$ is the plasma flow velocity, p is the thermal pressure, $\mathbf{B}$ is the magnetic field divided by $\sqrt{4\pi}$, e the total energy, E the internal energy, $\gamma = 5/3$ the rate of heat coefficients and η is the resistivity.

The software used in this work was in part developed by the ASC/Alliance Center for Astrophysical Thermonuclear Flashes at the University of Chicago (Fryxell et al. 2000). We perform 3D MHD simulations with the extensively validated FLASH4 code using the adaptive mesh refinement procedure (AMR) with the Powell's 8-wave scheme (Powell et al. 1999) to solve the MHD equations.

To generate a turbulent CS we start from a monolithic CS configuration with Lundquist value $S \gtrsim 10^{10}$, greater than the critical value ($S_c \sim 10^4$) at which the Sweet–Parker CS becomes unstable. In this way, a turbulent regime is generated giving account of a hi-

erarchical configuration of overdense plasma features connected by secondary CSs as described in the literature (see references in Priest and Forbes (2000)). The initial regime is set up with a uniform diffusivity of $\eta \approx 1\mathrm{m}^2\mathrm{s}^{-1}$, which is larger than the Spitzer value for a typical CS background temperature of $T = 10\mathrm{MK}$ ($\approx 0.03\mathrm{m}^2\mathrm{s}^{-1}$, $\eta \sim 10^9 T^{-3/2}\mathrm{m}^2\mathrm{s}^{-1}$ with $[T]$ =MK), yet lower than the estimated anomalous diffusivity (Bemporad 2008). We assume the CS parameters discussed above: $n = 2 \times 10^{10}\mathrm{cm}^{-3}$, $T = 10\mathrm{MK}$ and $B_0 = 5.9\mathrm{G}$. A Cartesian grid with 4 levels of refinement was employed leading to a maximum grid refinement of $(128, 256, 64)$. The physical domain was set up to $(50, 100, 25)\mathrm{Mm}$ (see right bottom corner of Figure 2), with the y coordinate pointing sunwards and the x and z coordinates perpendicular to the initial magnetic field direction. The basic CS device is initialized assuming a corona in pressure equilibrium with a velocity perturbation in the x direction given by

$$pert = v_0 \sin(2\omega y) \times random, \quad \omega = \frac{2\pi}{y_{max} - y_{min}}, \quad (10)$$

where $v_0 = 2\mathrm{km\,s}^{-1}$, *random* is a uniform distribution of numbers (varying between $(0 - 1)$) and $y_{max} - y_{min}$ is the domain size in the y direction. In addition to this perturbation, we consider various CS models with initial perturbed shear velocities (at $t = 0$s) in the y and z directions (see Table 1). The magnetic field configuration is:

$$B_y = \begin{cases} B_0 & \text{if } x < 0 \\ -B_0 & \text{if } x \geq 0 \end{cases} \quad (11)$$

where B_0 depends on the model. Periodic boundary conditions are assumed in the direction where a shear will be imposed (a $\mathbf{K}$ variable satisfies in direction n: $\mathbf{K}(n_{min}) = \mathbf{K}(n_{max})$ because no boundary effects are expected in the development of turbulence), otherwise outflow conditions are assumed.

6. Results and Discussion

A turbulent picture

From the initial conditions of the coronal plasma parameters (model $M0$ see Table 1) we obtain a turbulent configuration. Density slices of the $z = 0$ plane (edge-on view) are shown in Figure 2a–b for times: 20min and 40min, respectively. As shown in the figure, and extensively described in the literature, the tearing mode instability leads to a turbulent regime composed of dynamic and coalescent plasmoids where the desired subdense structures are only obtained as

Model	$B_0[G]$	$v_x[km\ s^{-1}]$	$v_y[km\ s^{-1}](x<0|x>0)$	$v_z[km\ s^{-1}](x<0|x>0)$	$(\Delta P/P)$
$M0$	5.9	*pert*	0|0	0|0	0
$M1$	5.9	*pert*	$(0|-364) + pert$	0|0	0
$M2$	0.59	*pert*	0|0	$(0|-182) + pert$	0
$M3$	5.9	*pert*	0|0	$(0|-364) + pert$	0
$M4$	5.9	*pert*	$(0|-364) + pert$	0|0	4

Table 1: Simulated models: B_0 is the background magnetic field, v_i is the initial velocities in the i direction, $x = 0$ is the position of the CS, $pert = v_0 \sin(2\omega y) \times random$ is the perturbation (same functional y dependence for all directions).

secondary linear CSs (they connect neighbor plasmoids). Thus, the usual tear–drop–shaped SAD features are not easy to obtain from models of the $M0$ type in times comparable to the observations.

However, if an instantaneous shear in the flow speed to the sides of the CS is introduced at $t = 0$s (models $M1$, $M2$ and $M3$ of Table 1), the turbulent features change markedly allowing the appearance of subdense cavities. It is well known that Kelvin–Helmholtz perturbations destabilize CSs (Bemporad 2008). When a shear initiates Kelvin–Helmholtz perturbations and combines with the tearing instability, the overall dynamic is modified. Accordingly, McKenzie (2013) reported strong coronal velocity shears (up to $\simeq [250 - 350]$km s^{-1}). Also, as large sunward flow values ($v_{flow} \simeq v_A \simeq [300 - 500]$km s^{-1}, v_A is the external Alfvén speed[1]) are expected coming from a reconnection site, strong shears in the flow could arise due to e.g. the inhomogeneities of the flaring medium (see e.g. the flow speed coming from the right side into the fan structure in slices between $11 : 58 : 09$ and $12 : 02 : 09$ of movie 1*b* by Savage et al. (2012)).

We thus perform several runs with initial strong shear velocities (see Table 1) to gain insight into the turbulent features. Figure 3 shows density slices of the $z = 0$ plane for $M1$, and for the same times as in Figure 2. The model configuration is the same as in $M0$ with the addition of a random speed with a shear in the y direction. Comparing Figure 3 and Figure 2 we note that models with shear can generate subdense cavities, lasting for times of the order of decades of minutes as the main features of the turbulent regime.

We also performed runs with a shear in the z direction (models $M2$ and $M3$). As in Figure 3, Figure 4a and Figure 4c show evolving subdense structures. The viewing orientation of Figure 4b and Figure 4d is, face-
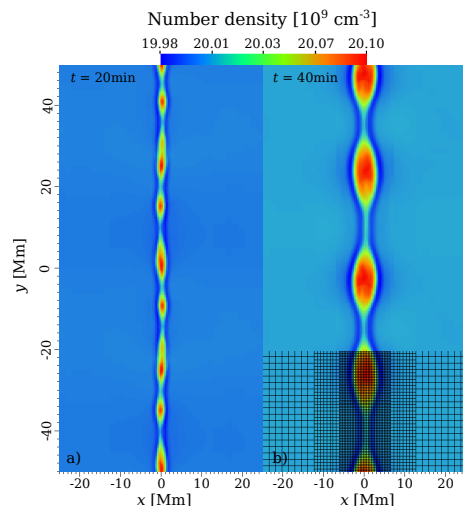

Fig. 2.— Simulation of $M0$, density slices of the plane $z = 0$ at a) $t = 20$min and b) $t = 40$min, superimposed we show the refinement of the grid.

on, perpendicular to the CS plane. These $x = 0$ plane descriptions resemble observational inhomogeneities as seen, for example, in movies 1*a* and 1*b*, or figure 1 by Savage et al. (2012). Nevertheless, these sunward subdense features are not stable during times comparable with the observation of that inhomogeneities, they cannot sustain their shape for more than 1.2min.

Later energy depositions

Once the turbulent CS is developed, we apply an instantaneous pressure pulse to emulate a blast reconnection event (Forbes 1988) occurring high in the corona where reconnection is prone to occur, triggered by a local change in the magnetic field line linkage and the magnetic topology, e.g., null points, separatrices or 3D quasi–separatrix layers, (see Demoulin et al. (1996)). Such initially localized processes that lead to bursts of impulsive deposition of energy that evolves produc-
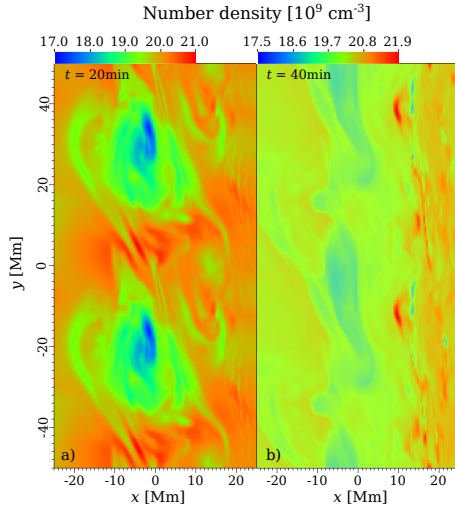
---

[1]v_A is the background Alfvén speed, where density and temperature have typical coronal values, e.g. considering $n = 10^9$cm^{-3} and $B_0 = 5.9$G, $v_A = 414$km s^{-1}.

Fig. 3.— Simulation of $M1$, density slices of the plane $z = 0$ at a) $t = 20$min and b) $t = 40$min.

ing an expansion of the plasma have been proposed in Scott et al. (2013); Cécere et al. (2012); Maglione et al. (2011); Costa et al. (2009). Also, the reconnection flare blast wave scenario was observationally confirmed by Kumar and Innes (2013), revealing the formation of initially expanding cavities that later collapse inwards while they approach an arcade, i.e., as they reach a supposedly denser medium.

Figure 5a–b shows one of these events (model $M4$) resulting from an instantaneous spherical pressure pulse that is four times its background value[2] at $t = 46.1$min. We assume a perturbation diameter of $d = 4$Mm located at $(0, 35, 0)$Mm leaving the medium density unaltered and allowing the increase of the internal temperature. The figure shows the $z = 0$ slice for the number density and the temperature at $t = 50.3$min. We obtain a tear–drop SAD that travels sunwards a distance of ~ 60Mm with a speed of ~ 240km s^{-1}, leaving a persistent voided region along a distance of ~ 38Mm. The fan number density is at least twice that of the SAD, and the SAD temperature
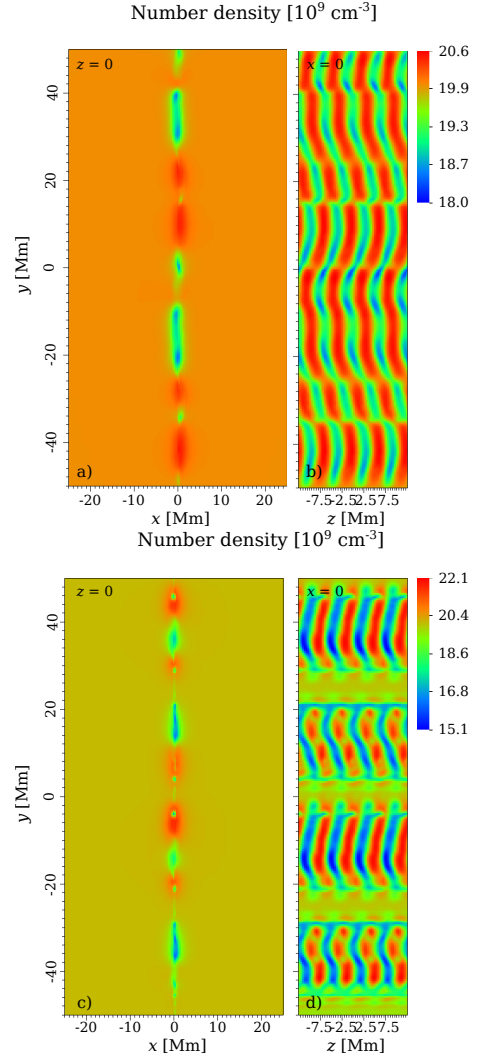

Fig. 4.— Simulation of model $M2$ at 8min, density slice: a) Edge-on view ($z = 0$) and b) Face-on view ($x = 0$). Simulation of model $M3$ at $t = 4.5$min, density slice: c) Edge-on and d) Face-on.

---

[2]This increase in the pressure can be produced e.g. by a burst reconnection of a stressed magnetic flux tube. To estimate the pressure pulse note that the temperature of a flaring loop can be as large as 40MK (Aschwanden 2005), and assuming that the density of the pulse is initially the same as the environment one, we obtain $\Delta P / P = \Delta T / T = 4$, considering that the fan CS temperature is of ≈ 10MK. The pressure pulse value could be larger if an increase of the density is also allowed, e.g., the number density of a flaring loop can be as high as $n \approx 10^{11}$cm^{-3}, much larger than the fan value considered.
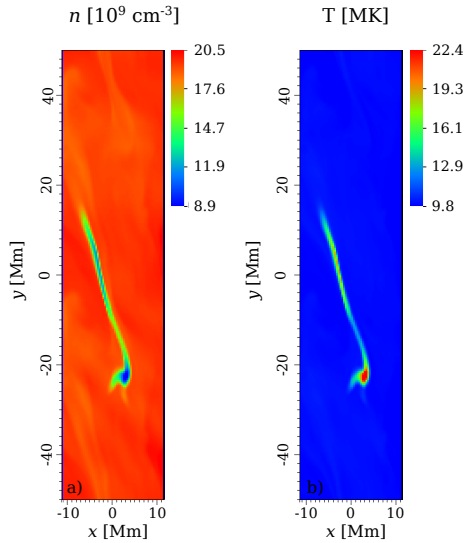
Fig. 5.— Slices of the $z = 0$ plane for Model $M4$ with a pressure pulse diameter of 4Mm, at $t = 50.3$min: a) number density, n and b) temperature, T. See also the movies attached to the electronic version of the paper.

is 22.4MK, whereas the number density of the turbulent background (Figure 3) is only ~ 1.23 times the eddy subdense cavities of temperature 10MK. In accordance with the observations (McKenzie 2013) our simulations show that the turbulent background has $\beta \geq 1$ values.

Dynamic behavior

To analyze the behavior of the subdense regions, we show in Figure 6a–b the $z = 0$ slice of the velocity (arrows), superimposed to the number density, for the turbulent vortice ($M1$) of Figure 3a and the SAD structure ($M4$) of Figure 5a, respectively. Figure 6c–d is as Figure 6a–b but the arrows are the magnetic field vector. As in McKenzie (2013) we obtain a variable spectrum of velocities and vortice–like frames which correlate with the motion of density depletions.

The initial β parameter value is ≈ 9 and, at later times, in the fan region, ranges between $\sim [3-100]$. In the vortical turbulent case (Figure 6a,c) the magnetic pressure is larger inside than outside the vortex and the gas pressure is almost constant ($\beta_{inside} < \beta_{outside} < 1$). As pointed out by McKenzie and Savage (2009); Savage and McKenzie (2011), Figure 6c suggests that the larger inside magnetic pressure could be the reason to avoid subdense cavities to be filled in immediately by
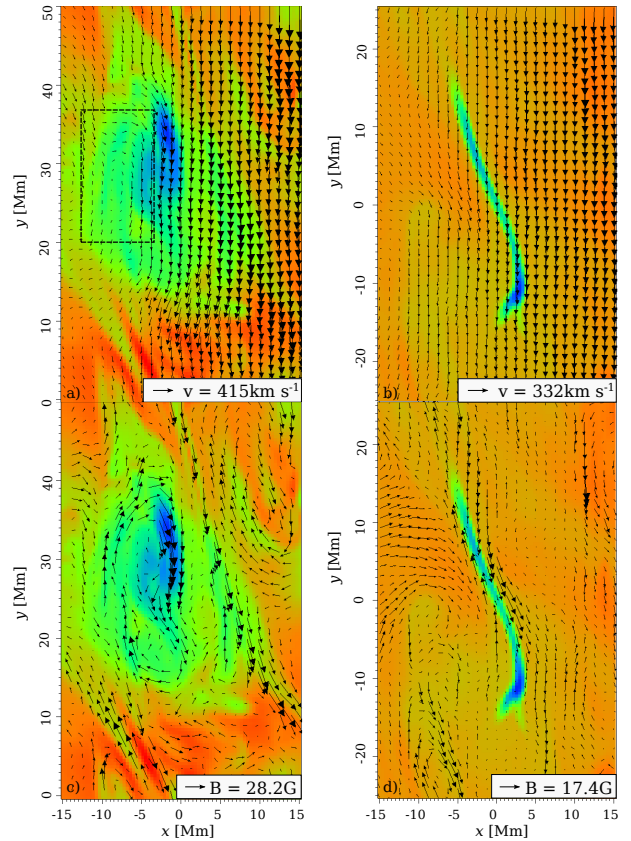

Fig. 6.— Velocity of the $z = 0$ view for models a) $M1$ at $t = 20$min and b) $M4$ at $t = 49.4$min. Magnetic field of the $z = 0$ view for models c) $M1$ at $t = 20$min and d) $M4$ at $t = 49.4$min. The arrows inserted represent values at the scale of the vector fields for the magnitude immediately to the lower right corner.

the surrounding plasma. Here, the cavities are the subdense eddies. On the contrary, the total pressure and the β parameter vary smoothly around the SAD features or are almost uniform (Figure 6b,d). Figure 6d shows that the magnetic field is larger outside than inside and, as in Cécere et al. (2012), the larger internal gas pressure –due to the large temperature values– resists the filling in of the SAD. This can also be watched from movies 1 and 2 where the triggering and the evolution of the density and temperature of a SAD is displayed. Note that the subdense SADs correspond to enhanced temperature values; the pressure is almost constant.

The eddy–like feature of size $\lesssim 20$Mm (indicated by a square in Figure 6a) has an average speed of 50km

8

s^{-1}. During the run we note the formation of eddies of sizes ranging between $\sim [10-20]$Mm and average speeds of $[10-60]$km s^{-1}. Unlike the interpretation done in Cécere et al. (2012), where the zigzag behavior is due to the interaction of SADs between each other and with the inhomogeneous medium, Figure 6b,d shows that the tail shape is produced by the interaction of a SAD with the turbulent fan.

The emission measure

To analyze if the subdense features seen in Figures 3 and 4 are compatible with a SAD description we first evaluate the emission measure (EM) (Aschwanden 2005) as:

$$EM = \int n^2 \, dx. \tag{12}$$

Figure 7 shows the EM of the face-on CS view for $M1$ and $M2$. The integration along the line of sight direction (x) is performed considering a CS width of 4Mm (see estimations in Guo et al. (2013)). The temperature range obtained is $\sim [9.4-10.8]$MK for these models. The weak contrast obtained for the EM –where the subdense cavities have EMs which are less than ~ 1.2 the background features– is lower than the reported by Savage et al. (2012) for $[10-13]$MK, where the EM SAD values were a factor of $[2-4]$ with respect to the surroundings (see Figure 4 of the mentioned paper). Larger width values (e.g. considering turbulent characteristic eddy sizes as ~ 22Mm) will lead to lower EM contrast values. Thus, the turbulent picture by itself is not sufficient to fully give account of dark observational regions.

Finally, Figure 8 shows the CS view of the emission measure at $t = 50.3$min for model $M4$. The EM is calculated along the line of sight considering the whole temperature range ($[10-22]$MK) and assuming a thickness of the CS of ~ 4Mm (Guo et al. 2013). At the initial times the SADs appear as rapidly increasing spherical features (e.g., see the high cadence movies of Savage et al. (2012)). Later, as shown in Figure 8, they acquire a tailed tear–drop shape while they are elongated and collimated by the turbulent background plasma. As stated in Savage et al. (2012), during times comparable with the observations (~ 270s), the SAD emission measure is approximately 2.1 times lower than its background value. However, if we consider a larger CS width the SAD EM contrast is insufficient to be appreciated.
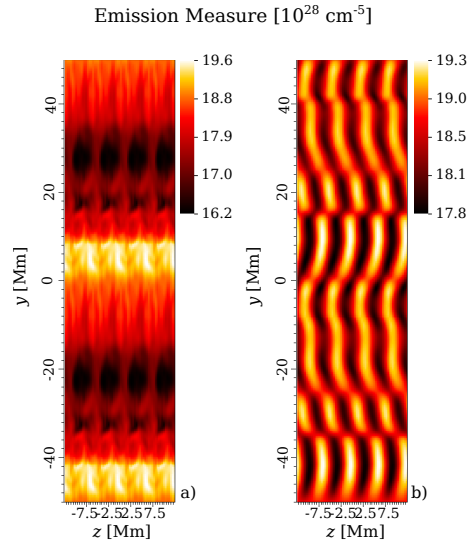

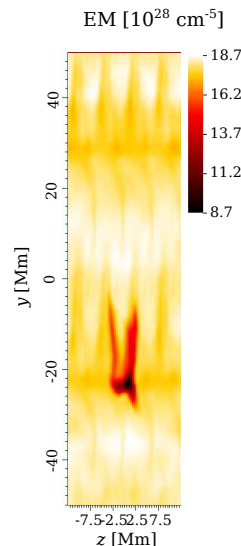Fig. 7.— Face-on view of EM for models a) $M1$ at 20min and b) $M2$ at 8min.

Fig. 8.— Face-on CS view of the EM for model $M4$, pulse size of $d = 4$Mm, at $t = 50.3$min.

Hence, we run the $M4$ model considering a CS thickness of 22Mm to obtain a SAD using the same instantaneous pressure pulse as before but with a larger diameter of 12Mm, located at $(0, 30, 0)$Mm and triggered at 27.5min. This value is in accordance with a rough estimation of the eddy width in Figure 3. Figure 9a-b shows the number density (with the superimposed arrows indicating the magnetic field) and

the temperature, respectively for the new run, at $t = 33$min. The subdense cavity (three times less than its background value, Figure 9a) sustains its structure for 5.5min tracing a path of 93Mm length. The sunward SAD velocity is ~ 280km s^{-1}. The eddies move with an average speed of ~ 40km s^{-1} at the neighbors of the SADs (McKenzie 2013). Figure 9b, shows larger SAD inside values of the temperature than the surrounding background. In Figure 10 we show the EM considering the mentioned thickness and a temperature threshold of $[10 - 20]$MK taking into account the AIA temperature filters which are not sensitive to temperature higher than 20MK (Boerner et al. 2012). Note that the EM contrast is sufficient (3.4) to be observed.
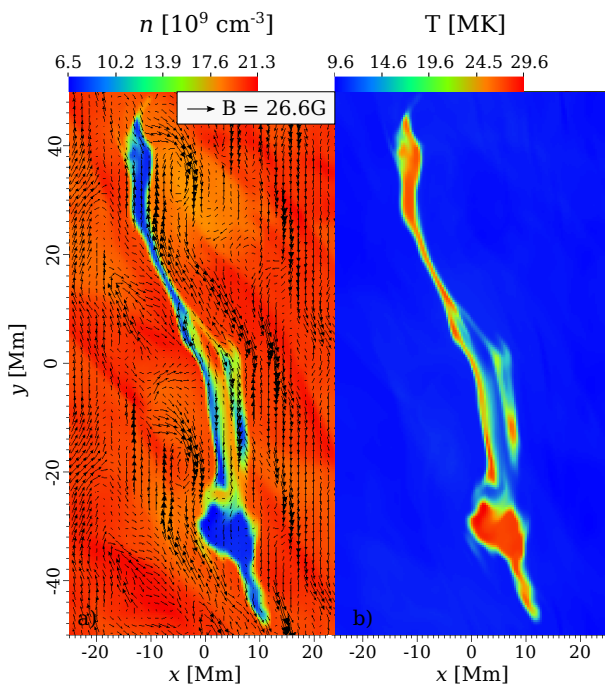

Fig. 9.— Slices of the $z = 0$ plane for Model $M4$ with a pressure pulse diameter of 12Mm, at $t = 33$min: a) number density with the arrows representing the magnetic field, n and b) temperature, T.

7. Conclusions

In this paper, motivated by recent CS observations (McKenzie 2013; Savage et al. 2012), we simulate a turbulent CS generated by a combination of the tearing and the Kelvin–Helmholtz instabilities, that develop subdense cavities with transient and variable vortical motions. While comparing these features with SAD
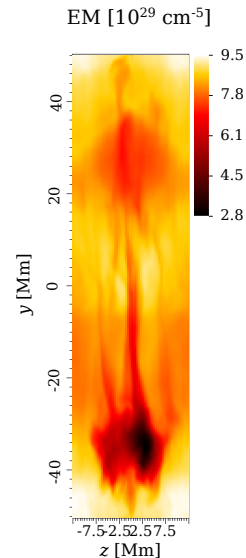

Fig. 10.— Face-on CS view of the EM for model $M4$, pulse size of $d = 12$Mm, at $t = 33$min.

observations we find that the EM contrast and the characteristic times are not enough to match the observations. However, imposing a pressure pulse to this turbulent background –in order to emulate a local deposition of energy produced by an impulsive reconnection event–, we obtain that –depending on the CS thickness–, the EM, the characteristic times and the speeds are comparable with the observations. If the CS is thin enough (~ 4Mm), the EM contrast will be sufficient to allow the detection of SADs. Thicker CSs (~ 22Mm) require larger depositions of energy to produce a detectable SAD. In both cases we use a triggering pressure pulse that is four times the background pressure, which is a reasonable value for a pressure perturbation in a flaring medium. In the first case, a $d = 4$Mm size is used to obtain a detectable EM, in the second one it was required an augmented flaring region of diameter $d = 12$Mm. These diameter values are typical SAD sizes.

Summarizing: for appropriated physical parameters, and a given pressure pulse intensity, it seems that there is a closed relation between characteristic SAD sizes and CS widths that must be satisfied to obtain an observable SAD. This could be a reason why SADs are not always detected during long duration flaring events.

In contrast with the results given by Hanneman and Reeves (2014), our simulated SAD temperatures

are always higher than the fan ones. These authors pointed out that there is little evidence that SADs contain substantially hotter plasma than the surrounding fan. Despite the actual SAD temperatures are significantly lower than in Maglione et al. (2011) and Cécere et al. (2012), we would like to emphasize that the scenario presented here (the scheme in Figure 1) may allow an explanation where the SAD temperature is not necessarily larger than the fan one. A more complex setup simulation where a SAD is triggered outside the fan region (Figure 1), may lead to a SAD with internal temperatures always higher than the surrounding background but not necessarily higher than the fan ones, e.g, if the background temperature is $T = 2$MK, and the fan temperature is $T = 10$MK, the SAD initial temperature will be $T = 8$MK, considering a pressure pulse of $\Delta P/P = 4$. In this case the SAD would enter the fan while it narrows and collapse due to the total pressure difference with the fan environment, as can be also seen in movie 1*b* by Savage et al. (2012).

Acknowledgment

REFERENCES

Aschwanden, M. J. (2005). *Physics of the Solar Corona. An Introduction with Problems and Solutions (2nd edition)*.

Bemporad, A. (2008). Spectroscopic Detection of Turbulence in Post-CME Current Sheets. *ApJ*, 689:572–584.

Boerner, P., Edwards, C., Lemen, J., Rausch, A., Schrijver, C., Shine, R., Shing, L., Stern, R., Tarbell, T., Title, A., Wolfson, C. J., Soufli, R., Spiller, E., Gullikson, E., McKenzie, D., Windt, D., Golub, L., Podgorski, W., Testa, P., and Weber, M. (2012). Initial Calibration of the Atmospheric Imaging Assembly (AIA) on the Solar Dynamics Observatory (SDO). *Sol. Phys.*, 275:41–66.

Cécere, M., Schneiter, M., Costa, A., Elaskar, S., and Maglione, S. (2012). Simulation of Descending Multiple Supra-arcade Reconnection Outflows in Solar Flares. *ApJ*, 759:79.

Ciaravella, A. and Raymond, J. C. (2008). The Current Sheet Associated with the 2003 November 4 Coronal Mass Ejection: Density, Temperature, Thickness, and Line Width. *ApJ*, 686:1372–1382.

Costa, A., Elaskar, S., Fernández, C. A., and Martínez, G. (2009). Simulation of dark lanes in post-flare supra-arcade. *MNRAS*, 400:L85–L89.

Demoulin, P., Henoux, J. C., Priest, E. R., and Mandrini, C. H. (1996). Quasi-Separatrix layers in solar flares. I. Method. *A&A*, 308:643–655.

Fermo, R. L., Drake, J. F., and Swisdak, M. (2010). A statistical model of magnetic islands in a current layer. *Physics of Plasmas*, 17(1):010702.

Forbes, T. G. (1988). Shocks produced by impulsively driven reconnection. *Sol. Phys.*, 117:97–121.

Fryxell, B., Olson, K., Ricker, P., Timmes, F. X., Zingale, M., Lamb, D. Q., MacNeice, P., Rosner, R., Truran, J. W., and Tufo, H. (2000). FLASH: An Adaptive Mesh Hydrodynamics Code for Modeling Astrophysical Thermonuclear Flashes. *ApJS*, 131:273–334.

Guo, L.-J., Bhattacharjee, A., and Huang, Y.-M. (2013). Distribution of Plasmoids in Post-coronal Mass Ejection Current Sheets. *ApJ*, 771:L14.

Hanneman, W. J. and Reeves, K. K. (2014). Thermal Structure of Current Sheets and Supra-arcade Downflows in the Solar Corona. *ApJ*, 786:95.

Heyvaerts, J. and Kuperus, M. (1978). The triggering of plasma turbulence during fast flux mergence in the solar corona. *A&A*, 64:219–234.

Innes, D. E., McKenzie, D. E., and Wang, T. (2003a). Observations of 1000 km s^{-1} Doppler shifts in 10^7 K solar flare supra-arcade. *Sol. Phys.*, 217:267–279.

Innes, D. E., McKenzie, D. E., and Wang, T. (2003b). SUMER spectral observations of post-flare supra-arcade inflows. *Sol. Phys.*, 217:247–265.

Kumar, P. and Innes, D. E. (2013). Multiwavelength Observations of an Eruptive Flare: Evidence for Blast Waves and Break-Out. *Sol. Phys.*, 288:255–268.

Lazarian, A. and Vishniac, E. T. (1999). Reconnection in a Weakly Stochastic Field. *ApJ*, 517:700–718.

Linton, M. G., Devore, C. R., and Longcope, D. W. (2009). Patchy reconnection in a Y-type current sheet. *Earth, Planets, and Space*, 61:573–576.

Maglione, L. S., Schneiter, E. M., Costa, A., and Elaskar, S. (2011). Simulation of dark lanes in post-flare supra-arcades. III. A 2D simulation. *A&A*, 527:L5.

McKenzie, D. E. (2000). Supra-arcade Downflows in Long-Duration Solar Flare Events. *Sol. Phys.*, 195:381–399.

McKenzie, D. E. (2013). Turbulent Dynamics in Solar Flare Sheet Structures Measured with Local Correlation Tracking. *ApJ*, 766:39.

McKenzie, D. E. and Hudson, H. S. (1999). X-Ray Observations of Motions and Structure above a Solar Flare Arcade. *ApJ*, 519:L93–L96.

McKenzie, D. E. and Savage, S. L. (2009). Quantitative Examination of Supra-arcade Downflows in Eruptive Solar Flares. *ApJ*, 697:1569–1577.

Onofri, M., Primavera, L., Malara, F., and Veltri, P. (2004). Three-dimensional simulations of magnetic reconnection in slab geometry. *Physics of Plasmas*, 11:4837–4846.

Powell, K. G., Roe, P. L., Linde, T. J., Gombosi, T. I., and De Zeeuw, D. L. (1999). A Solution-Adaptive Upwind Scheme for Ideal Magnetohydrodynamics. *Journal of Computational Physics*, 154:284–309.

Priest, E. and Forbes, T. (2000). *Magnetic Reconnection*.

Priest, E. R. (1982). *Solar magneto-hydrodynamics*.

Priest, E. R. (1986). Magnetohydrodynamic theories of solar flares. *Sol. Phys.*, 104:1–18.

Priest, E. R. and Démoulin, P. (1995). Three-dimensional magnetic reconnection without null points. 1. Basic theory of magnetic flipping. *J. Geophys. Res.*, 100:23443–23464.

Savage, S. L. and McKenzie, D. E. (2011). Quantitative Examination of a Large Sample of Supra-arcade Downflows in Eruptive Solar Flares. *ApJ*, 730:98.

Savage, S. L., McKenzie, D. E., and Reeves, K. K. (2012). Re-interpretation of Supra-arcade Downflows in Solar Flares. *ApJ*, 747:L40.

Schmieder, B., Aulanier, G., Demoulin, P., van Driel-Gesztelyi, L., Roudier, T., Nitta, N., and Cauzzi, G. (1997). Magnetic reconnection driven by emergence of sheared magnetic field. *A&A*, 325:1213–1225.

Schulz, W., Costa, A., Elaskar, S., and Cid, G. (2010). Simulation of dark lanes in post-flare supra-arcades - II. A contribution to the remote sensing of the coronal magnetic field. *MNRAS*, 407:L89–L93.

Schwenn, R., Raymond, J. C., Alexander, D., Ciaravella, A., Gopalswamy, N., Howard, R., Hudson, H., Kaufmann, P., Klassen, A., Maia, D., Munoz-Martinez, G., Pick, M., Reiner, M., Srivastava, N., Tripathi, D., Vourlidas, A., Wang, Y.-M., and Zhang, J. (2006). Coronal Observations of CMEs. Report of Working Group A. *Space Sci. Rev.*, 123:127–176.

Scott, R. B., Longcope, D. W., and McKenzie, D. E. (2013). Peristaltic Pumping near Post-coronal Mass Ejection Supra-arcade Current Sheets. *ApJ*, 776:54.

Seaton, D. B. and Forbes, T. G. (2009). An Analytical Model for Reconnection Outflow Jets Including Thermal Conduction. *ApJ*, 701:348–359.

Somov, B. V., Titov, V. S., and Verneta, A. I. (1987). Magnetic reconnection in solar flares. *Itogi Nauki i Tekhniki Seriia Astronomiia*, 34:136–237.

Verwichte, E., Nakariakov, V. M., and Cooper, F. C. (2005). Transverse waves in a post-flare supra-arcade. *A&A*, 430:L65–L68.